Atomic Structure of Interconnected Few-Layer Graphene Domains

Alex W. Robertson,[†] Alicja Bachmatiuk,[‡] Yimin A. Wu,[†] Franziska Schäffel,[†] Bernd Rellinghaus,[‡] Bernd Büchner,[‡] Mark H. Rümmeli,[‡,§] and Jamie H. Warner[†,*]

[†]Department of Materials, University of Oxford, Parks Road, Oxford OX1 3PH, United Kingdom, [‡]IFW Dresden, P.O. Box 270116, D-01171 Dresden, Germany, and [§]Technische Universität Dresden, D-01062 Dresden, Germany

ABSTRACT The atomic structure at the boundary interface between interconnected few-layer graphene (FLG) domains, synthesized by atmospheric pressure chemical vapor deposition (AP-CVD), is examined using aberration-corrected high-resolution transmission electron microscopy. Moiré patterns in the HRTEM images reveal the presence of rotational stacking faults in the boundary region that extend over distances of ~100 nm. We show that FLG domains interconnect *via* two principle processes: graphene sheets from one domain grow over the top of a neighboring domain, while other graphene domains interconnect by direct atomic bonding. Differentiating between these two types of interconnects was found to be possible by examining the HRTEM contrast profiles produced at the interface. Graphene sheets that terminate were found to produce strong edge contrast with increasing defocus values, as well as a broader edge cross section, whereas atomically bonded interfaces were found to not exhibit any contrast, even under large defocus values. These findings are reinforced by correlating with multi-slice TEM image simulations of appropriate structures.

KEYWORDS: graphene · chemical vapor deposition · CVD · aberration-corrected TEM · grain boundary

The novel electronic properties of graphene, such as the relativistic motion of their charge carriers, marks it out as a material of interest for several applications, such as transparent conducting films.[1−3] The ability to synthesize large-area graphene by chemical vapor deposition (CVD)[4,5] allows for the prospect of a viable route to incorporation into commercial products. The growth of graphene on a nickel catalyst has been shown to yield FLG,[4] with copper-catalyzed growth favoring a self-limiting monolayer.[5] Graphene films synthesized by CVD are of a polycrystalline nature, with multiple small graphene domains growing to merge into a continuous film.[6] Aberration-corrected high-resolution transmission electron microscopy (AC-HRTEM) allows for the detailed study of the atomic structure of graphene[7] and can be combined with the analysis and filtering of 2D fast Fourier transforms (FFT) to generate reconstructed images that can be used to elucidate the stacking configuration of the graphene layers.[8] Understanding the atomic structure of polycrystalline graphene synthesized by CVD may assist in the further development of the field;[9−11] for instance, the use of graphene domain boundaries may allow for the engineering of the band structure,[12] and electronic devices have shown increased resistivities for inter-domain electronic transport when compared to intradomain measurements, with weak localization also observed in the inter-domain case.[13]

As shown schematically in Figure 1, there are two primary ways one can envisage two separate graphene domains being connected: either by direct atomic bonding at the interface of the two graphene sheets to create a discrete atomic domain boundary (Figure 1a,b) or by one sheet overlapping another to form a bilayer boundary region that is not atomically discrete and relies on interlayer van der Waals forces to hold the two domains together (Figure 1c,d). These shall be referred to as the atomic interface and the overlap interface, respectively. Recent investigations of monolayer graphene domain boundaries reported the existence of atomically bonded discrete interfaces.[14,15] These domain boundaries were found to consist of pentagonal, hexagonal, and heptagonal carbon rings connected in a chain, allowing for two graphene domains of different lattice directions to bond together.

In a previous report, we showed that hexagonal single-crystal domains of FLG could be produced on the surface of copper foils using atmospheric pressure CVD.[16] In the cases where the FLG domains merged together to form a polycrystalline film, 2D mapping of the FLG domain's crystallographic orientations, using selected area electron diffraction (SAED), showed random orientations. Some regions of the polycrystalline FLG film showed multiple reflections in the SAED patterns (*i.e.*, at least two graphene lattices with some arbitrary rotation),

* Address correspondence to jamie.warner@materials.ox.ac.uk.

Received for review June 3, 2011 and accepted July 22, 2011.

Published online August 05, 2011
10.1021/nn202051g

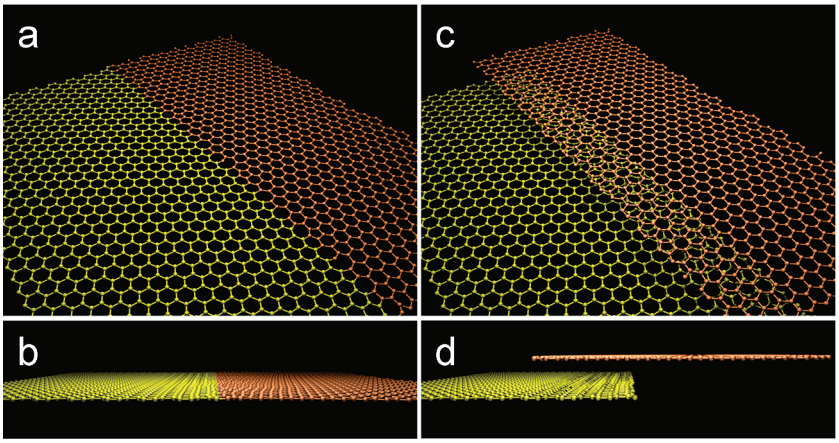

Figure 1. Schematic illustrations of the two primary ways of connecting graphene sheets. (a) Three-dimensional perspective view of atomic bonding at the interface. (b) Side view of the atomic interface. (c) Three-dimensional perspective view showing the graphene sheet on the right overlapping on top of the graphene sheet on the left (*i.e.*, overlap interface). (d) Side view of the overlapping interface.

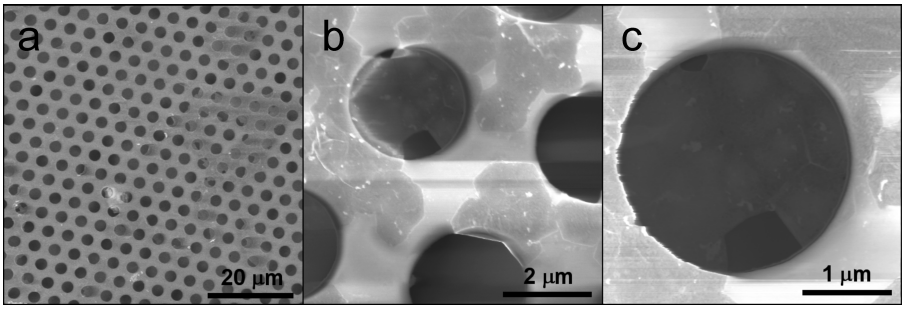

Figure 2. SEM images of a holey silicon nitride membrane TEM grid after graphene transfer. Graphene coverage of the viewing holes was only evident in a limited number of cases.

and it is unclear whether this is due to contributions from two single crystals with different orientations or from a region that contains rotational stacking faults. SAED is limited in its spatial resolution, and as such, other techniques are required to gain information about the origin of the multiple reflections in the SAED patterns and thus the true nature of the domain boundaries in these films. Here we present an investigation of the atomic structure of the domain boundaries between FLG domains using aberration-corrected HRTEM at an accelerating voltage of 80 kV.

RESULTS AND DISCUSSION

Samples were grown using CVD and transferred onto holey silicon nitride (Si_3N_4, but abbreviated to SiN) membrane TEM grids for electron microscopy characterization (see the Method Details section). Scanning electron microscopy (SEM) imaging of the SiN membrane TEM grid was conducted after FLG transfer in order to confirm successful adhesion of the film and to provide insight into the degree of folding and distortion induced from the process. Figure 2a demonstrates that the majority of the holes in the SiN membrane are not covered by the FLG. This is attributed to the small domain size (~1 μm) of the FLG obtained under the used growth conditions,[16] as these are smaller than the membrane holes one could expect that the adhesion between adjacent domains may not always be sufficient to allow for them to bridge the hole. However, as can be seen in Figure 2b,c, some holes in the SiN membrane are covered by FLG, allowing for the possibility of TEM inspection.

Figure 3a shows a TEM image of a region of the sample where two FLG domains have merged together. Inspection of this area using HRTEM with a magnification high enough to observe the atomic structure enabled the layer stacking orientations to be tracked across this region. Regions with pure AB Bernal stacking gave rise to a hexagonal lattice structure, while regions containing rotational stacking faults produced Moiré patterns. Figure 3b–f shows five examples of HRTEM images taken from the five regions marked with boxes in Figure 3a. The respective 2D fast Fourier transform (FFT) is shown as an inset in each image. The six-fold crystal symmetry of graphene results in the 2D FFT having a set of six hexagonally distributed spots with 0.21 nm lattice spacing in the first ring. The orientation of the spots in the FFT is directly related to the armchair direction of the graphene lattice.[17] A rotational stacking fault in the

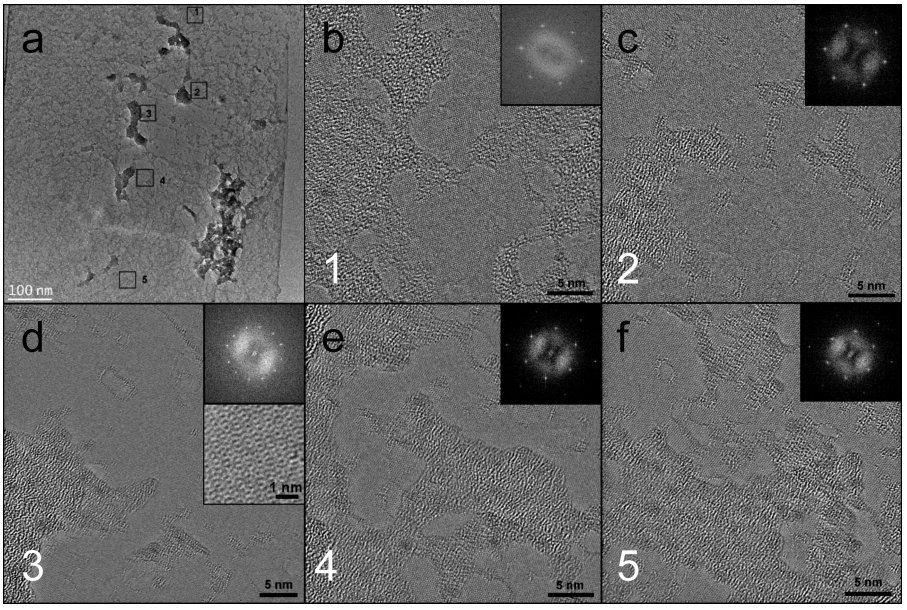

Figure 3. (a) Low-magnification TEM image of a region of FLG, with the 2D FFT taken from the numbered boxed regions. (b–f) HRTEM images from the appropriately labeled boxed regions in (a); insets show the 2D FFT pattern. Additional inset for (d) shows the Moiré interference pattern that can be observed at high magnification in area 3.

few-layer graphene adds another six spots to this inner ring, due to the rotation of the graphene lattice direction with respect to the original lattice direction. If the rotational stacking fault is intrinsic to the layer order (*i.e.*, not from a back-fold), then this is likely to be a turbostratic configuration. The FFT spots from regions 1 and 2 (Figure 3b,c) share the same direction, as do regions 4 and 5 (Figure 3e,f). Region 3, where the Moiré pattern is observed in the real space image (Figure 3d), exhibits a superposition of region 1–2 and region 4–5, which when compared with the location shown in Figure 3a suggests that region 3 bestrides a boundary between two graphene domains of different crystal orientations. The typical scale of the turbostratic region between these two domains was found to be on the order of 100 nm by scanning the region for observable Moiré patterns using HRTEM. This indicates that the domain boundary is not atomically defined and provides context to the selected area electron diffraction (SAED) we recently reported.[16]

Even though the Moiré pattern, and thus the boundary region, between two FLG domains is on the order of 100 nm, we were able to find regions on the extremities of this boundary that exhibited sharp transitions from AB stacking to Moiré patterns. As was discussed in Figure 1, there are two possible ways that the graphene layers can connect. In order to evaluate whether HRTEM can distinguish between these two interfaces, we performed HRTEM image simulations to examine their resulting contrast profiles. A comparison of the differences between the two would enable the reliable identification of the boundary type.

Figure 4a shows a top view of an incomplete sheet of graphene (yellow) residing on three sheets of graphene with AB Bernal stacking (gray), with a lattice direction mismatch of approximately 23° between the two. This is representative of the connectivity shown in Figure 1c, the overlap interface, where one graphene sheet with non-AB orientation overlaps another set of AB stacked FLG sheets. HRTEM image simulations are shown in Figure 4b–d for increasing levels of defocus (5, 10, and 40 nm, respectively). The Moiré interference pattern originating from the rotational stacking fault from the incomplete layer is visible in the top half of the images, while the hexagonal pattern expected from AB Bernal FLG can be found on the bottom. A negative mask filter was applied to the FFT of Figure 4d and inverted to reconstruct an image without the respective contribution of one of the two lattices, as shown in Figure 4e,f, with the masks shown in the insets. Figure 4e shows a rotated hexagonal pattern along the top half and thus is the incomplete layer contribution, while Figure 4f yields a continuous lattice stretching across the image and can be concluded to be the AB Bernal contribution. It was apparent that the contrast of the boundary increased concomitantly with the defocus, as did the boundary breadth, which can be readily identified qualitatively by inspection of Figure 4b–e. Figure 4g shows a portion of a reconstructed image generated by removing all of the periodic lattice components from Figure 4d. Figure 4h shows an intensity box profile taken from the region indicated with a red box, with pixel values along the *x*-axis summed to give one average gray value and then plotted as a function of the distance in the *y*-axis. The minimum gray value in Figure 4h is 179, with a maximum at 197, thus giving a total difference of 18 gray scale units across the profile.

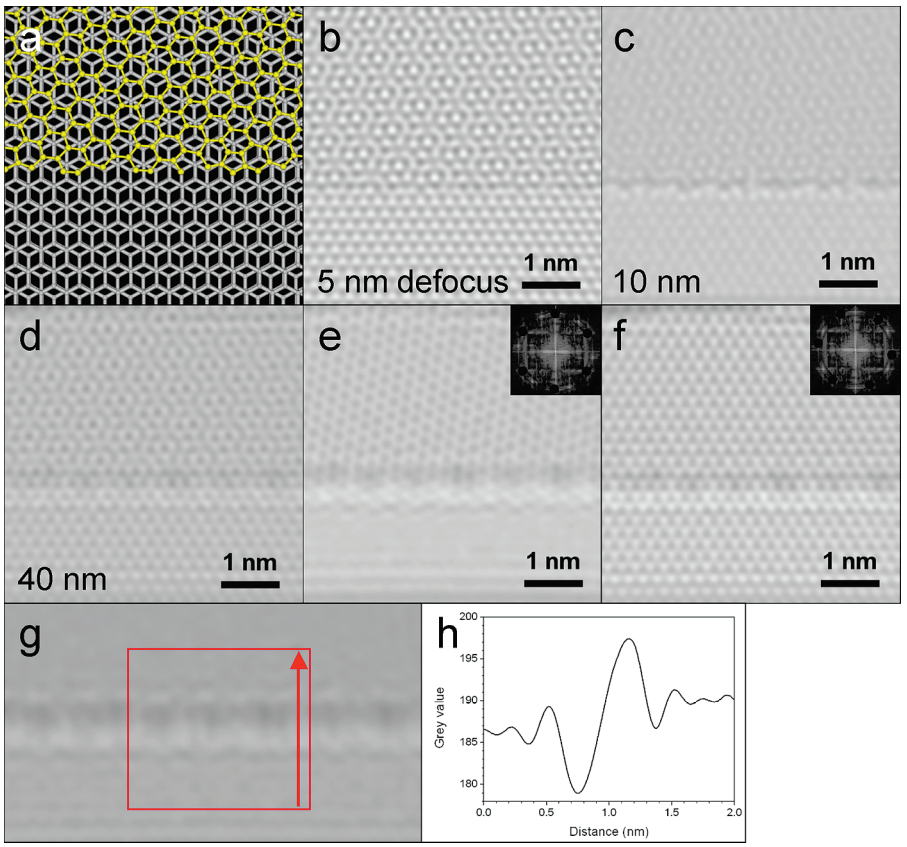

Figure 4. (a) Top-down view of the graphene overlap interface used in the simulation, showing the underlying AB Bernal stacked graphene (gray) and a rotationally mismatched upper layer across part of the structure (yellow). (b–d) Electron microscopy image simulations of (a) at 5, 10, and 40 nm defocus, respectively, taken in the region of the sheets termination. (e,f) Reconstructed images from the FFT negative masks, shown in the respective insets, taken from the 40 nm defocus simulation. (g) Close up of the boundary of a reconstructed image from both FFT negative masks of the 40 nm defocus simulation. (h) Box profile taken vertically of the red region in (g).

Figure 5a illustrates a top-down view of an atomically bonded interface between two graphene lattices of different orientations (yellow), on top of three graphene layers with AB Bernal stacking (gray). This is the representative of the connectivity shown in Figure 1a, the atomic interface. The bottom half of the top graphene layer adopts AB stacking with the underlying FLG. Image simulations (Figure 5b–d) for defocus values of 5, 10, and 40 nm, respectively, show a similar Moiré pattern on top of a hexagonal base as in Figure 4, and this is further demonstrated in the reconstructions shown in Figure 5e,f. The principle difference between the two cases lies in the behavior of the boundary. Figure 5g shows a portion of a reconstructed image of Figure 5d after all of the periodic lattice structure was removed by an FFT mask. Figure 5h shows an intensity box profile, taken from the red box region in Figure 5g. Variation in gray values of 182–185 units gives a difference of 3 units over the box plot range, with no discernible boundary edge seen.

Comparing the intensity profiles presented in Figure 5h with Figure 4h reveals a significant difference between the two types of connectivity. It is apparent that the principle identifier for differentiating between an overlapping, incomplete graphene sheet and an atomically bonded graphene interface is the level of contrast of the boundary. Specifically, in the case of an atomic bonding interface between two graphene sheets, it was noted that there was negligible contrast at the boundary. However, for the overlap interface, it was found that there was a significant contrast change in the region of the edge and that also the breadth of the boundary was found to increase with defocus, an effect not observed for the atomically bonded interface.

Utilizing this information, it was possible to identify the two types of graphene interfaces with HRTEM. Figure 6 shows a high-magnification HRTEM image of an atomic interface between two graphene sheets of different lattice rotations. In Figure 6a, a Moiré interference pattern can be seen on the left of the image, indicating the presence of a rotational stacking fault, and the hexagonal patterning on the right shows AB Bernal stacked FLG. Further analysis by applying a FFT was performed, yielding the expected sets of hexagonal spots. In the inset for Figure 6a, the FFT shows two sets of hexagonal spots at 0.21 nm lattice spacing, confirming the presence of a rotational stacking fault.

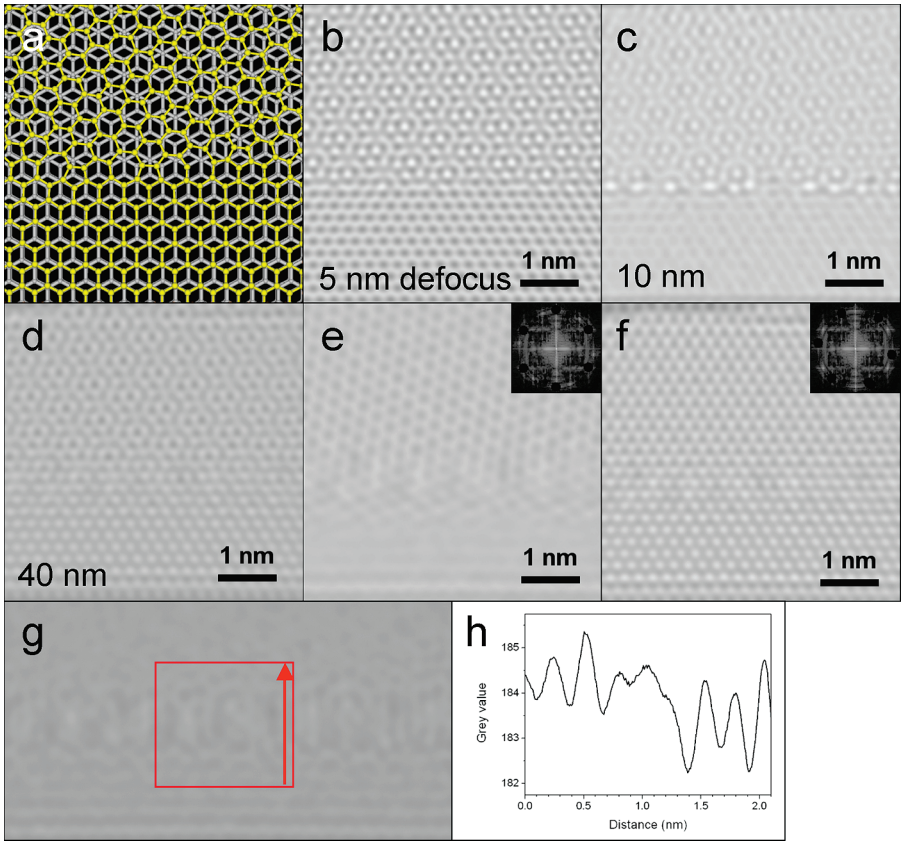

Figure 5. (a) Top-down model of an atomically bonded interface between an AB Bernal layer and a rotationally mismatched partial single layer (yellow), on top of AB Bernal graphene (gray). (b–d) Electron microscope simulations of (a) at 5, 10, and 40 nm defocus, respectively, taken in the region of the graphene interface. (e,f) Reconstructed images from the FFT negative masks, shown in the respective insets, taken from the 40 nm defocus simulation. (g) Close up of the boundary of a reconstructed image from both FFT negative masks of the 40 nm defocus simulation. (h) Box profile taken vertically of the red region in (g).

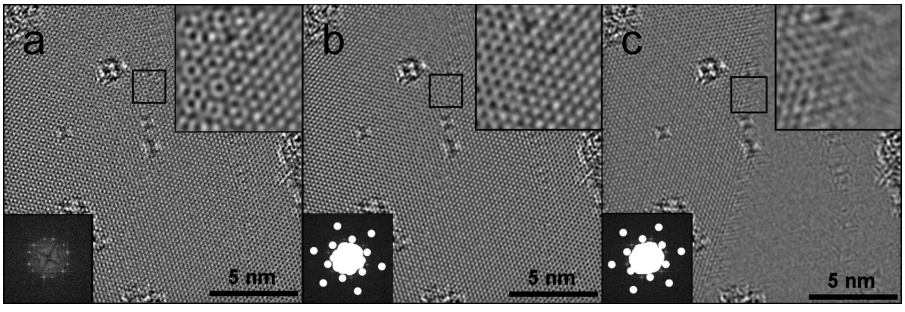

Figure 6. (a) HRTEM image of a graphene interface taken at a low defocus, with insets showing the FFT (lower left) and a magnified view of the boxed region (upper right). (b,c) Images reconstructed from the frequency domains selected by the positive masks shown in the lower left of each.

Figure 6b,c shows the reconstructed images from the inclusive masks shown in the lower left insets. The high-magnification images located at the top right of Figure 6a–c are taken from each of the boxed regions and are used to highlight the change in the real space image across the boundary. From these insets, it can be confirmed that the boundary is of an atomic interface type, due to the expected lack of contrast along the edge. Variation of the defocus yielded no change in the contrast of the interface (see Supporting Information).

Figure 7 shows a further example of a HRTEM image taken from another area, with a similar boundary region showing Moiré patterns on one side and AB Bernal stacked FLG on the other. However, this region demonstrates both an atomically bonded interface and an overlapping region and, as such, can be used to directly compare the two. In the lower left (yellow) of Figure 7a, the Moiré interference associated with turbostratic graphene is evident, which arises from the graphene layer shown by the application of the

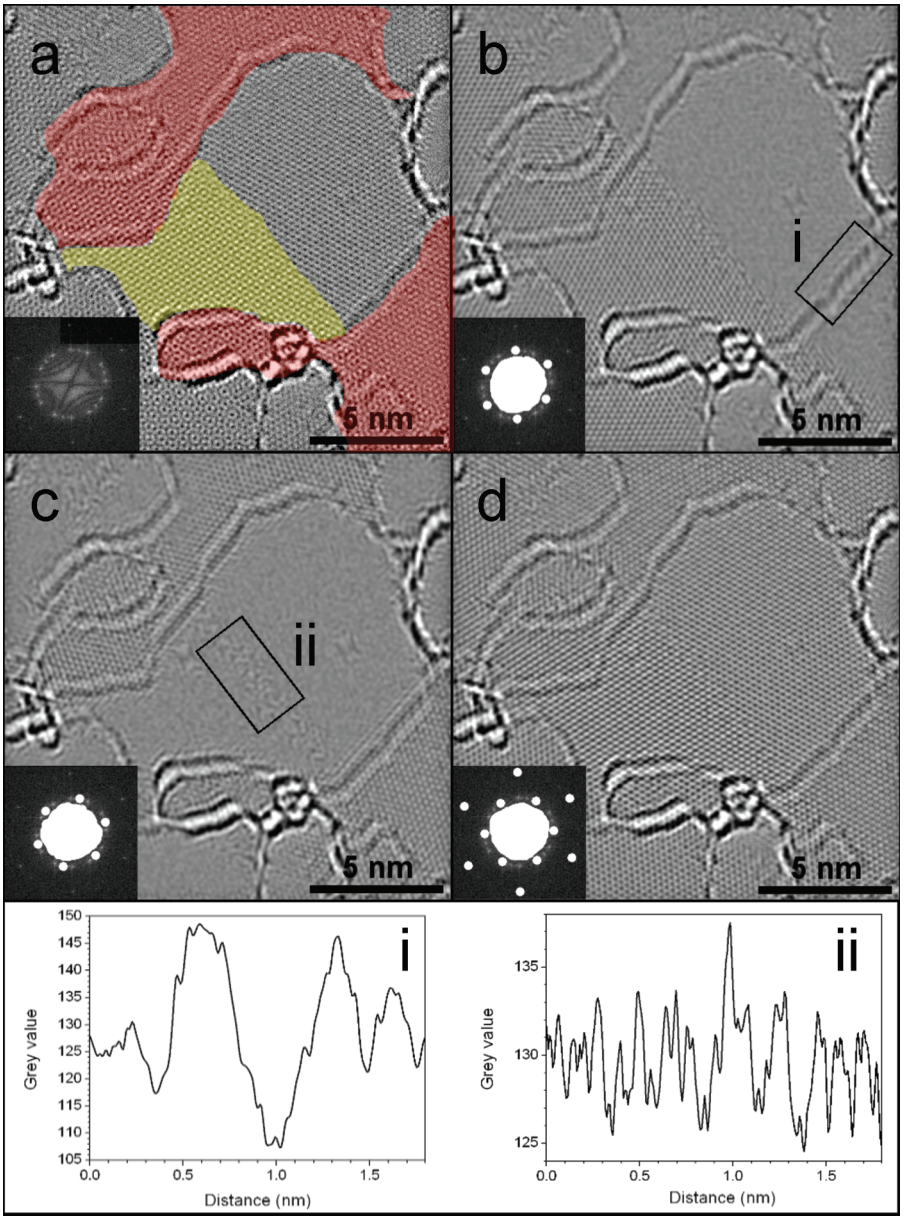

Figure 7. HRTEM image of several graphene sheets overlaying one another. The image was taken at a defocus of approximately 40 nm. The lower left inset shows an FFT taken from the image. (b–d) Reconstructed images from the frequency domains selected in the insets. (i,ii) Box averaged intensity profiles across the appropriately labeled boxed regions in (b) and (c).

positive mask used in Figure 7b. Reconstruction of the FFT positive mask in Figure 7d shows the underlying AB stacked FLG, with the remaining set of diffraction spots, shown in Figure 7c, accounted for by graphene about the periphery (red). The texturing of the FLG sheet in this area is due to the sputtering from the 80 kV electron beam during the extensive periods of imaging.[18,19] However, this was not observed to affect the graphene atomic interface. The edge from the sheet giving rise to the central Moiré pattern can be seen to have negligible contrast variation, in comparison to the remainder of the graphene edges around the perimeter; these lead to the reconstructed graphene planes in Figure 7c and the second Moiré patterns at the bottom right and top left in Figure 7a, which exhibit a strong contrast and a broad extent when imaged under a defocus of approximately 40 nm. Thus the central boundary can be concluded to be an atomically bonded interface, whereas the higher contrast boundaries about the periphery are of the overlap interface type. Figure 7c also illustrates a feature that was found for all boundaries studied: that elimination of both the constituent graphene lattice contributions to the image by FFT reconstruction does not lead to the entire removal of the contrast from the edge. The likely reason for the edge still being visible is that it is composed of various defects: randomly orientated pentagons, hexagons, and heptagons in the case of

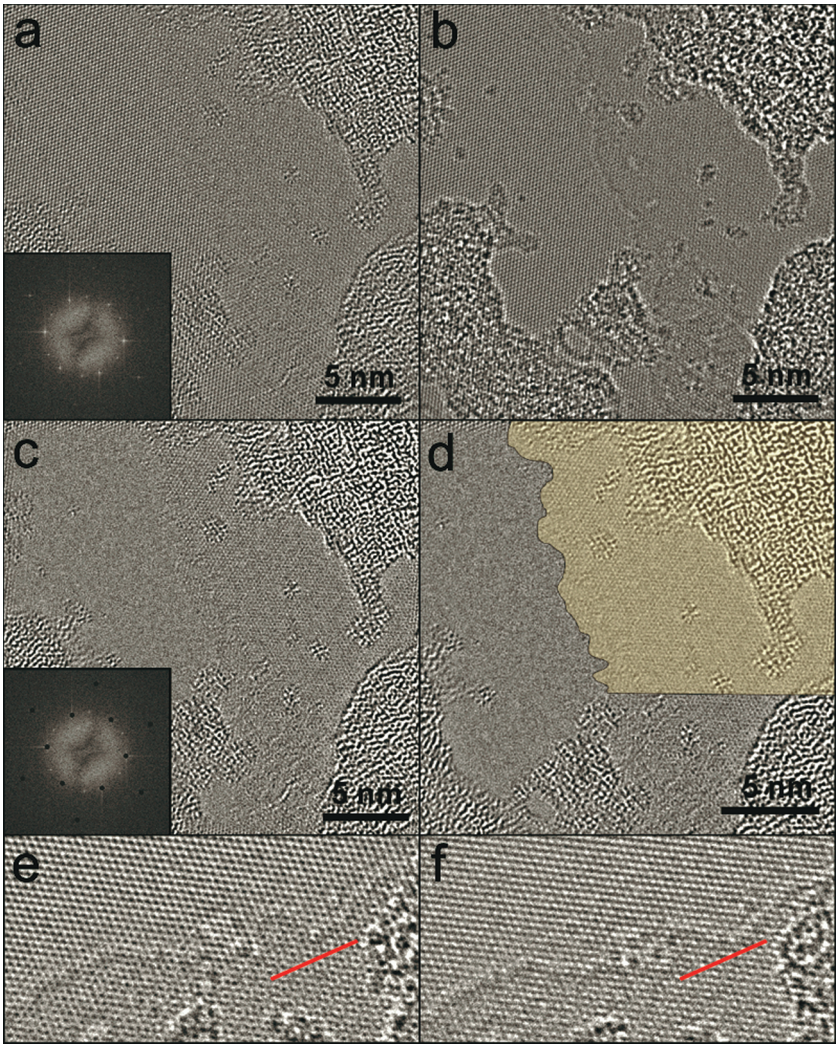

Figure 8. (a) Low defocus HRTEM image of a region containing an overlap interface; the inset shows the FFT. (b) Same region as (a), taken under high defocus. (c) Reconstructed image from the negative mask shown in the inset, showing the partial sheet on the right of the image which generated the Moiré pattern in (a). (d) Overlay of the edge, taken from (b), matched on to (d). (e) Magnified and rotated image taken from the box in (b). (f) Same region as (e) taken after a 10 s exposure to the electron beam.

the atomic bonding interface and electron beam irradiation damaged edges in the case of the incomplete sheet. Since these defects would not likely be aligned with either of the two lattice directions, the reconstruction from the FFT mask would not lead to their removal, and thus they would be expected to remain. Labels i and ii in Figure 7 are box averaged intensity profiles across the appropriately annotated boxed regions in panels b and c. Further intensity profiles are presented in the Supporting Information.

The image simulations demonstrated a marked increase in contrast for the overlapping graphene edges when the magnitude of the defocus was increased. Figure 8a shows another overlap interface, with the Moiré pattern visible on the right. A subsequent image was taken with increased defocus, with the extra contrast emphasizing the edge. Comparing this to the reconstructed image from the negative mask FFT (Figure 8c), one finds that they correlate well, as shown by the overlay in Figure 8d. The boundary is rough, with an approximate variation of between 0.5 and 1 nm from the average line. This differs with the comparably smooth and straight boundaries seen for the atomic interfaces shown in Figures 6 and 7. The roughness could be attributed to the action of incident electrons from the electron beam.[18] Figure 8f shows a further image taken at a similar defocus to panel b (Figure 8e is a magnified and rotated image of the appropriate region from panel b) and shows some change in the profile of the boundary due to electron beam sputtering, in particular, along the area of the boundary denoted by the red line. No such variation was observed for the atomic interfaces in Figures 6 and 7. Variations in the susceptibility of electron-beam-induced sputtering have been observed for intrinsic graphene edges compared to folded graphene edges

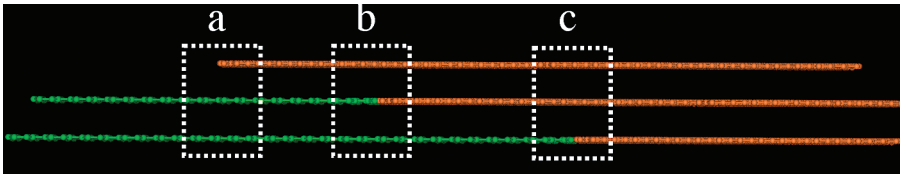

Figure 9. Schematic illustration showing the side view of two neighboring few-layer graphene domains intersecting (green, bilayer; orange, trilayer). Region (a) shows the top layer of the trilayer graphene domain (orange) overlapping onto the bilayer graphene domain (green), which in HRTEM would result in a Moire pattern on the right and hexagonal structure typical of AB Bernal graphite on the left. Region (b) shows an atomically bonded interface in the middle, which would result in a Moire pattern on both the left and right side. Region (c) shows an atomically bonded interface in the bottom layer, which would result in a Moire pattern on the left and hexagonal structure on the right.

due to the presence of unsaturated atoms terminated intrinsic graphene edges.[20]

The presence of these two distinct interface types is likely to be contingent on the system being of several layers. The atomic interface, much as for monolayer graphene, occurs when two graphene sheets in the same plane grow into one another. The inevitable rotational mismatch of the lattice directions between the two domains is resolved by the formation of five- and seven-membered carbon rings along the boundary. The nature of the overlap interface is more complex. The models in Figures 1 and 4 show a sheet of graphene that is overlaying an AB ordered graphene structure, with a rotational mismatch, and that terminates part way. It has been shown in our previous work[16] that FLG grown on copper by CVD, in general, does not adopt a turbostratic configuration, thus the rotational mismatch of the boundary cannot be explained by incomplete turbostratic layers growing on top of the underlying graphene structure. It is possible that under certain circumstances when two adjacent FLG domains grow into one another this overlap may be observed. For atomic interfaces to form, it would require that the graphene sheets from the adjacent domains be suitably aligned in the axis perpendicular to the sheet. Thus, if one of the domains was thicker than its neighbor, it is possible that the sheets on top may continue to grow across the adjacent domain, with the crystal structure of these higher sheets matching its original seed domain rather than that of the neighbor. This is illustrated schematically in Figure 9.

CONCLUSION

Graphene domain boundaries and the interconnection between FLG sheets are important considerations when working to optimize electronic and mechanical properties. The ability to identify domain boundaries, and differentiating them from isolated sheet edges, is potentially important for electronic device fabrication. The mechanical strength of polycrystalline 2D films of FLG could be improved by reducing the number of overlapping sheets at the interfaces between individual FLG domains, as only van der Waals forces provide the adhesion, in contrast to atomically bonded domains that have stronger covalent bond attachments. Image simulations and AC-HRTEM imaging demonstrate that there are two discernible types of graphene boundaries in the FLG system, where one is the case of the termination of a graphene layer on top of another and the second the case of an atomically bonded graphene–graphene interface between two sheets of different lattice directions. It is possible to differentiate between the two graphene boundaries by observing the variation in contrast over the cross section of the boundary, with the size of the cross section increasing concomitantly with the defocus for the overlapping graphene layer case, and with little discernible edge contrast for the atomic graphene interface scenario. The presented images and observations illustrate the complexity of the FLG system, with both atomic domain boundaries and small regions of turbostratic graphene, originating from overlap at domain intersections, in an otherwise well-ordered AB Bernal stacked graphitic system.

METHOD DETAILS

FLG was synthesized according to a previously reported method.[16] Copper foils (Alfa Aesar, product no. 42189, 99.999% purity) were loaded into a quartz tube located in a horizontal split-tube furnace. After purging the system with argon gas, 600 sccm of a hydrogen/argon gas mix (25% hydrogen) was introduced into the system. At a temperature of 1000 °C, the quartz tube was shifted inward into the furnace, so that the sample resided in the hot zone, where it was annealed and reduced for 30 min to remove surface oxide. A methane/argon gas mixture (20% methane), with a flow rate of approximately 5–10 sccm, was then supplied, while continuing to maintain the 600 sccm hydrogen gas mix flow, for 3 min. The sample was cooled to ambient temperature by shifting the quartz tube from the furnace and was left to rapidly cool under a hydrogen and argon atmosphere.

For transfer of graphene from the copper foils, an A8 PMMA supportive scaffold (8 wt % in anisole, 495k molecular weight) was spin coated on to the graphene surface. A spin speed of 4700 rpm was used for 60 s, with the film then cured by heating at 180 °C for 90 s. The underlying copper was etched away overnight by an iron(III) chloride solution (concentration of 0.1 g mL^{-1}). The graphene/PMMA film was then rinsed in deionized water and transferred to a concentrated hydrochloric acid

solution (30%), in order to remove residual contaminants, such as iron from the etching solution. A further thorough rinsing in DI water was then performed. Transfer of the film to a holey silicon nitride TEM grid (Agar Scientific number Y5385) was done by attaching the grid to a lightly sticky pad (Gel-Pak gel-film WF-40-X8-A), which in turn was attached to a glass slide, and using this to "scoop" the film out of the DI water. A further coating of A8 PMMA was applied by drop casting; this acts to relax the graphene film on to the TEM grid, allowing for better adhesion and a better quality transfer of the graphene.[21] This was allowed to dry in air over several hours. The PMMA can be then removed by first applying acetone solvent, and then by baking in air for 2−3 h at about 350 °C.

SEM images were taken with a Zeiss NVision 40 FIB-SEM operating an accelerating voltage of 2 kV. The AC-HRTEM presented in Figure 4 was performed using an aberration-corrected JEOL 2010F microscope operating at 80 kV. The AC-HRTEM presented in Figures 6−8 was performed using an aberration-corrected FEI Titan^3 80−300 microscope operated at 80 kV. Beam current densities were typically in the range of ~0.0001−0.01 pA nm^{-2}.

Image simulations were performed using the multi-slice algorithm in JEMS software using a supercell (90 × 80 × 20 nm), with a defocus spread of 8 nm, C_s = −0.005 mm, and defocus ranging from 5 to 40 nm, as stated in the text.

Acknowledgment. J.H.W. thanks the Royal Society for funding. F.S. thanks the Alexander von Humboldt foundation, the BMBF, and the EPSRC (EP/F048009/1). A.B. thanks the Alexander von Humboldt foundation. M.H.R. thanks the EU (ECEMP) and the Freistaat Sachsen.

Supporting Information Available: The effect of image defocus on contrast and further box averaged intensity profiles of boundaries are shown in supplementary figures. This material is available free of charge *via* the Internet at http://pubs.acs.org.

REFERENCES AND NOTES

1. Novoselov, K. S.; Geim, A. K.; Morozov, S. V.; Jiang, D.; Katsnelson, M. I.; Grigorieva, I. V.; Dubonos, S. V.; Firsov, A. A. Two-Dimensional Gas of Massless Dirac Fermions in Graphene. *Nature* **2005**, *438*, 197–200.
2. Novoselov, K. S.; Geim, A. K.; Morozov, S. V.; Jiang, D.; Zhang, Y.; Dubonos, S. V.; Grigorieva, I. V.; Firsov, A. A. Electric Field Effect in Atomically Thin Carbon Films. *Science* **2004**, *306*, 666–669.
3. Novoselov, K. S.; Morozov, S. V.; Mohinddin, T. M. G.; Ponomarenko, L. A.; Elias, D. C.; Yang, R.; Barbolina, I. I.; Blake, P.; Booth, T. J.; Jaing, D.; *et al.* Electronic Properties of Graphene. *Phys. Status Solidi B* **2007**, *244*, 4106–4111.
4. Kim, K. S.; Zhao, Y.; Jang, H.; Lee, S. Y.; Kim, J. M.; Kim, K. S.; Ahn, J. H.; Kim, P.; Choi, J. Y.; Hong, B. H. Large-Scale Pattern Growth of Graphene Films for Stretchable Transparent Electrodes. *Nature* **2009**, *457*, 706–710.
5. Li, X.; Cai, W.; An, J.; Kim, S.; Nah, J.; Yang, D.; Piner, R.; Velamakanni, A.; Jung, I.; Tutuc, E.; *et al.* Large-Area Synthesis of High-Quality and Uniform Graphene Films on Copper Foils. *Science* **2009**, *324*, 1312–1314.
6. Li, X.; Magnuson, C. W.; Venugopal, A.; An, J.; Suk, J. W.; Han, B.; Borysiak, M.; Cai, W.; Velamakanni, A.; Zhu, Y.; *et al.* Graphene Films with Large Domain Size by a Two-Step Chemical Vapor Deposition Process. *Nano Lett.* **2010**, *10*, 4328–4334.
7. Hashimoto, A.; Suenaga, K.; Gloter, A.; Urita, K.; Iijima, S. Direct Evidence for Atomic Defects in Graphene Layers. *Nature* **2004**, *430*, 870–873.
8. Warner, J. H.; Rümmeli, M. H.; Gemming, T.; Büchner, B.; Briggs, G. A. D. Direct Imaging of Rotational Stacking Faults in Few Layer Graphene. *Nano Lett.* **2009**, *9*, 102–106.
9. Grantab, R.; Shenoy, V. B.; Ruoff, R. S. Anomalous Strength Characteristics of Tilt Grain Boundaries in Graphene. *Science* **2010**, *330*, 946–948.
10. Yazyev, O. V.; Louie, S. G. Topological Defects in Graphene: Dislocations and Grain Boundaries. *Phys. Rev. B* **2010**, *81*, 195420.
11. Malola, S.; Häkkinen, H.; Koskinen, P. Structural, Chemical, and Dynamical Trends in Graphene Grain Boundaries. *Phys. Rev. B* **2010**, *81*, 165447.
12. Yazyev, O. V.; Louie, S. G. Electronic Transport in Polycrystalline Graphene. *Nat. Mater.* **2010**, *9*, 806–809.
13. Yu, Q.; Jauregui, L. A.; Wu, W.; Colby, R.; Tian, J.; Su, Z.; Cau, H.; Liu, Z.; Pandey, D.; Wei, D.; *et al.* Control and Characterization of Individual Grains and Grain Boundaries in Graphene Grown by Chemical Vapour Deposition. *Nat. Mater.* **2011**, *10*, 443–449.
14. Kim, K.; Lee, Z.; Regan, W.; Kisielowski, C.; Crommie, M. F.; Zettl, A. Grain Boundary Mapping in Polycrystalline Graphene. *ACS Nano* **2011**, *5*, 2142–2146.
15. Huang, P. Y.; Ruiz-Vargas, C. S.; van der Zande, A. M.; Whitney, W. S.; Levendorf, M. P.; Kevek, J. W.; Garg, S.; Alen, J. S.; Hustedt, C. J.; Zhu, Y.; *et al.* Grains and Grain Boundaries in Single-Layer Graphene Atomic Patchwork Quilts. *Nature* **2011**, *469*, 389–393.
16. Robertson, A. W.; Warner, J. H. Hexagonal Single Crystal Domains of Few-Layer Graphene on Copper Foils. *Nano Lett.* **2011**, *11*, 1182–1189.
17. Warner, J. H.; Schäffel, F.; Rümmeli, M. H.; Büchner, B. Examining the Edges of Multi-layer Graphene Sheets. *Chem. Mater.* **2009**, *21*, 2418–2421.
18. Warner, J. H.; Rümmeli, M. H.; Ge, L.; Gemming, T.; Montanari, B.; Harrison, N. M.; Büchner, B.; Briggs, G. A. D. Structural Transformations in Graphene Studied with High Spatial and Temporal Resolution. *Nat. Nanotechnol.* **2009**, *4*, 500–504.
19. Girit, C. O.; Meyer, J. C.; Erni, R.; Rossell, M. D.; Kisielowski, C.; Yang, L.; Park, C.-H.; Crommie, M. F.; Cohen, M. L.; Louie, S. G.; *et al.* Graphene at the Edge: Stability and Dynamics. *Science* **2009**, *323*, 1705–1708.
20. Warner, J. H.; Rümmeli, M. H.; Bachmatiuk, A.; Büchner, B. Examining the Stability of Folded Graphene Edges Against Electron Beam Induced Sputtering with Atomic Resolution. *Nanotechnology* **2010**, *21*, 325702.
21. Li, X.; Zhu, Y.; Cai, W.; Borysiak, M.; Han, B.; Chen, D.; Piner, R. D.; Colombo, L.; Ruoff, R. S. Transfer of Large-Area Graphene Films for High-Performance Transparent Conductive Electrodes. *Nano Lett.* **2009**, *9*, 4359–4363.